IET Intelligent Transport Systems

Research Article

IET Journals
The Institution of Engineering and Technology

Cooperative adaptive cruise control in mixed traffic with selective use of vehicle-to-vehicle communication

ISSN 1751-956X
Received on 10th September 2017
Revised 12th May 2018
Accepted on 9th July 2018
E-First on 28th August 2018
doi: 10.1049/iet-its.2018.5235
www.ietdl.org

Linjun Zhang[1] ✉

[1]*Department of Mechanical Engineering, University of Michigan, Ann Arbor, MI 48109, USA*
✉ *E-mail: linjunzh@umich.edu*

Abstract: This study is focused on the design of cooperative adaptive cruise control (CACC) to regulate the longitudinal motion of connected and automated vehicles (CAVs) in mixed traffic that is composed of human-driven vehicles and CAVs. Wireless vehicle-to-vehicle communication is exploited to monitor the motion of multiple broadcasting vehicles, and a strategy is designed to determine whether the received data of other vehicles are incorporated into CACC. A condition is derived for choosing control gains that ensure the internal stability of CAVs in the presence of time delays and switching connectivity topologies of information flow. Moreover, because the switching connectivity topologies may change the dynamics of the whole vehicle chain, the authors apply a data-driven approach for online optimisation of control gains such that CACC adapts to the variations of connectivity topologies. The proposed selective CACC is validated through numerical simulations. To enhance the fidelity of simulations, they use the data collected through on-road experiments to simulate the motion of human-driven vehicles and apply the physics-based vehicle dynamic model to simulate the motion of CAVs. Simulation results demonstrate the advantages of the proposed selective CACC in improving vehicle safety and in mitigating perturbations in mixed traffic.

1 Introduction

The ground transportation system plays an important role in the modern society. However, the dramatically growing number of vehicles has caused problems such as traffic congestions and vehicle collisions. These problems are typically caused by the limited perception capability and the large reaction time of human drivers. By using range sensors (e.g. radar and lidar) to monitor the distance and the relative velocity with respect to the vehicle immediately ahead, adaptive cruise control (ACC) was designed to regulate the longitudinal motion of vehicles, in order to enhance vehicle safety and to improve passengers' comfort [1]. However, the improvement of the ACC on traffic efficiency is not significant since the applied sensors can only monitor the motion of the vehicles within the line of sight.

Nowadays, the emerging wireless vehicle-to-vehicle (V2V) communication technology can be exploited to monitor the motion of vehicles beyond the line of sight. This has great potential for enhancing vehicle safety, improving traffic efficiency, and reducing fuel consumption. In practice, V2V communication can be realised by applying the dedicated short-range communication (DSRC) [2, 3], which provides high-speed data transmission for communication-based active safety applications. Integrating V2V communication into automated vehicles leads to the concept of connected and automated vehicles (CAVs), and the cooperative ACC (CACC) is proposed to regulate the longitudinal motion of CAVs by incorporating the information received from V2V communication [4]. According to whether the implementation allows the incorporation of human-driven vehicles, CACC can be divided into two categories: CACC platooning and CACC in mixed traffic. CACC platooning requires all participant vehicles to be automated vehicles and it aims to optimise the performance of the whole platoon. A large number of studies have shown the benefits of CACC platooning in increasing traffic capacity and reducing fuel consumption by allowing small inter-vehicle distances and by attenuating perturbations [5–9]. The impacts of CACC platooning on the improvement of traffic dynamics were also demonstrated by experimental projects such as California PATH [10], SARTRE [11], GCDC [12], and experiment on heavy-duty trucks [13]. However, in near future, the penetration of automated vehicles in daily traffic may not be high enough for the implementation of CACC platoons on general roads.

The traffic in the near future may be mixed by conventional human-driven vehicles that do not broadcast information, advanced human-driven vehicles that broadcast information, and CAVs. This motivates the research on CACC in mixed traffic. The study in [14] showed that CACC can improve the dynamics of mixed traffic flow even when the penetration of CAVs is low. In [15], a hierarchical control architecture was proposed for reducing the complexity of CACC design in the presence of uncertain vehicle dynamics and external disturbances. The effects of nonlinear dynamics and time delays on CACC performance in mixed traffic were investigated in [16–18], while optimal CACC was studied in [19]. All these studies on CACC in mixed traffic were based on non-selective strategies. That is, the motion data of other vehicles received from V2V communication are always incorporated into CACC. Although non-selective CACC has potential for reducing collision risks when distant broadcasting vehicles brake sharply, they also impose additional accelerations on CAVs when distant broadcasting vehicles accelerate, which may cause safety problems, especially when there are non-broadcasting human-driven vehicles between the broadcasting vehicle and the CAV. For example, consider the scenario shown in Fig. 1 (best viewed in colour online) where vehicles 0 and 1 accelerate, vehicle 2 decelerates for turning, and vehicle 3 monitors the motion of vehicles 0 and 2 by range sensors and/or V2V communication. If vehicle 3 exploits non-selective CACC, it may collide with vehicle 2, because the acceleration of vehicle 0 pulls vehicle 3 to accelerate when vehicle 3 should decelerate to avoid the collision.

To deal with the aforementioned safety issue, in this study, we investigate selective CACC in mixed traffic, which results in three main contributions. First, a strategy is designed for the selective use of the information provided by V2V communication, in order to enhance the safety of CACC in mixed traffic. Then, a condition is derived for choosing control gains that guarantee the internal stability of CAVs in the presence of varying gains and switching connectivity topologies. Finally, we propose a data-driven approach for online optimisation of control gains without requiring the knowledge about the dynamics of other vehicles, which is particularly useful for mixed traffic that includes human-driven vehicles.

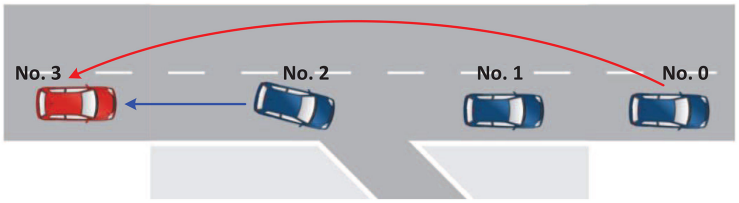

Fig. 1 *A traffic scenario where vehicles 0 and 1 accelerate while vehicle 2 decelerates for turning. Here, vehicle 3 is a CAV that monitors the motion of vehicles 0 and 2, while vehicle 1 does not broadcast information. The arrows indicate the directions of information flow, where the short-range link (blue) can be realised by range sensors or V2V communication while long-range links (red) can only be realised through V2V communication since distant vehicles are typically beyond the line of sight*

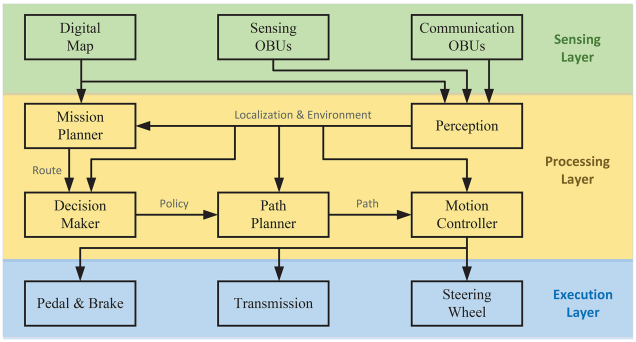

Fig. 2 *System configuration of CAVs*

The rest of this paper is arranged as follows. In Section 2, the system configuration of CAVs is briefly introduced and a selective CACC strategy is presented to determine whether the information received from V2V communication is used in CACC. Section 3 is focused on the design of control gains, where a condition for internal stability is presented and a data-driven approach is applied for online optimisation of control gains. In Section 4, numerical simulations are conducted to compare the performance of the selective CACC and that of the non-selective CACC. Finally, we conclude the results and discuss future research directions in Section 5.

2 Selective CACC in mixed traffic

In this section, a general system configuration of CAVs is introduced, and a CACC strategy is presented to regulate the longitudinal motion of CAVs by selectively incorporating the motion data of broadcasting vehicles received from V2V communication. Throughout this study, we focus on the mixed traffic composed of human-driven vehicles that neither broadcast nor receive information, human-driven vehicles that only broadcast information, and CAVs that broadcast information and also utilise the received information in longitudinal motion control.

2.1 System configuration of CAVs

CAV systems are typically constructed by three layers as demonstrated in Fig. 2, where the arrows indicate the directions of information flow. The *sensing layer* monitors the environment around CAVs and it includes a digital map, sensing on-board units (OBUs), and communication OBUs. The digital map contains information about the road network topologies, locations of traffic signs (e.g. traffic light and stop/yield sign), and traffic rules (e.g. speed limit). Sensing OBUs usually include sensors like global positioning system (GPS), inertial measurement unit (IMU), camera, radar, and lidar for localising the ego vehicle and monitoring the surrounding objects. Communication OBUs are used for information exchange among traffic participants such as vehicles, infrastructure, and pedestrians.

The *processing layer* processes the raw data provided by the sensing layer and determines the control commands for the motion of CAVs. The perception module localises the ego vehicle on the digital map, and it also comprehends the surrounding environment through object detection, classification, and tracking. After the CAV receives a destination, the mission planner exploits the digital map and plans a route to the destination. Based on the route and the surrounding environment, the decision maker determines the policy (e.g. lane keeping/change, turn left/right, yield, overtake etc.). The path planner takes the policy given by the decision maker and generates a collision-free path accordingly. Finally, the motion controller calculates the inputs to the actuators (e.g. pedal, brake, steering wheel etc.) in the *execution layer* such that the vehicle can track the desired path. Note that Fig. 2 only presents the basic layers and modules of CAV systems. In practice, it may vary for different CAVs.

2.2 Selective CACC

According to the planned route and the surrounding environments, the decision maker determines the optimal policy from a variety of policies, which include *yielding* for the cut-in vehicles, *keeping* the current lane, *overtaking* slow vehicles, *changing* to the left/right lane, *turning* left/right, and many other policies. Each of these policies may correspond to a specific control strategy. In particular, when the CAV aims to keep the current lane, a steering control is applied for lane keeping, and CACC is applied to regulate the longitudinal motion, either following the vehicles ahead or maintaining the speed limit when there are no vehicles ahead. In this study, we assume that there is a steering controller that maintains the vehicle in the lane [20] and hence focus on the design of CACC.

CACC exploits V2V communication to monitor the motion of broadcasting vehicles, even those beyond the line of sight. In practice, V2V communication can be realised through the DSRC, which transmits basic safety messages (BSMs) to support active safety applications. According to the SAE J2735 Message Set Dictionary standard [21], BSMs are comprised of two parts where Part I includes state information of the broadcasting vehicle such as position, speed, heading, and vehicle size; see Table 1 for details. For the implementation of CACC, we first transform the global coordinate (latitude and longitude) to the local s–e coordinate where s denotes the longitudinal distance along the centreline of the lane and e is the lateral deviation from the centreline. For structured roads, the digital map provides a sequence of waypoints that represent the centreline location and the heading of each lane. By matching the global coordinate and the heading of CAV with those of waypoints, one can project the vehicle in the certain lane on the digital map with lateral error e. The distance s along the centreline can be accumulated from the predefined origin where $s = 0$. Typically, CACC only incorporates the motion data of the

Table 1 SAE J2735 standard for DSRC BSM Part I [21]

Data item name	Description
DSRC_MessageID	the first element in every message, used by the parser to determine how to parse the rest of the message
MsgCount	a sequence number, incremented with each successive transmission of a BSM, used primarily to estimate packet error statistics
TemporaryID	a value chosen randomly and held constant for a few minutes, it helps a receiver correlate a stream of BSMs from a sender
DSecond	the current time, modulo one minute, with resolution 1 ms
latitude and longitude	geographic latitude and longitude, with resolution 1/10 microdegree
elevation	position above or below sea level, resolution 0.1 m
PositionAccurary	conveys the one-standard-deviation position error along both semi-major and semi-minor axes, and the heading of the semi-major axis
TransmissionAndSpeed	vehicle transmission (gear) setting and unsigned vehicle speed with resolution 1 cm/s
heading	compass heading of vehicle's motion, resolution 1/80°
SteeringWheelAngle	current position of the steering wheel, resolution 1.5°. Clockwise rotation is positive
AccelerationSet4Way	longitudinal acceleration, lateral acceleration, vertical acceleration, and yaw rate
BrakeSystemStatus	conveys whether or not braking is active on each of four wheels
VehicleSize	vehicle length and width, resolution 1 cm

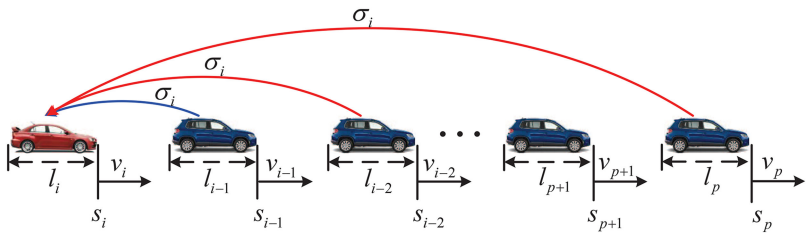

Fig. 3 *A vehicle chain where vehicle i (red) is a CAV that receives information from multiple vehicles ahead. Vehicle p denotes the furthest broadcasting vehicle within the communication range of vehicle i. s_j, l_j, and v_j denote position, length, and velocity of vehicle j, respectively. σ_i is used to denote the information delay*

vehicles that are in the same lane with the receiving CAV. Another important factor for integrating V2V communication in CACC is clock synchronisation among all vehicles. In practice, the local clocks of vehicles can be synchronised to the coordinated universal time through the GPS receiver, or they can be synchronised with the precision time protocol through a computer network [22].

Fig. 3 (best viewed in colour online) shows a vehicle chain where vehicle i is a CAV that monitors the position s_j and the velocity v_j of broadcasting vehicle j, where vehicle p denotes the furthest broadcasting vehicle within the communication range of vehicle i. The symbol l_j denotes the length of vehicle j. The motion of the vehicle immediately ahead can be monitored by range sensors (e.g. radar and lidar) or V2V communication, while the motion of distant vehicles can only be monitored by using V2V communication since these vehicles are beyond the line of sight. σ_i represents the information delay, which is caused by intermittency of sensors or V2V communication. In practice, the value of σ_i can be obtained by comparing the time stamp of the received data and the clock of the receiving CAV.

To design CACC, we consider a simplified model

$$\begin{aligned} \dot{s}_i(t) &= v_i(t), \\ \dot{v}_i(t) &= u_i(t), \end{aligned} \tag{1}$$

where the acceleration u_i is to be designed to determine the position s_i and velocity v_i by incorporating the motion data of broadcasting vehicles received from V2V communication. The corresponding results can be implemented in vehicles as a high-level controller through the hierarchical control architecture presented in [15], where a low-level controller is provided to regulate engine torque and brake such that the vehicle states track the desired states generated by (1) in the presence of uncertainties and disturbances (see Fig. 4).

In general, CACC can be designed in the form

$$u_i(t) = \sum_{j=p}^{i-1} \gamma_{i,j} f_{i,j}(s_j(t-\sigma_i), s_i(t-\sigma_i), v_j(t-\sigma_i), v_i(t-\sigma_i)), \tag{2}$$

where the switch coefficient $\gamma_{i,j}$ is used to determine whether the motion data received from vehicle j are used by vehicle i, the function $f_{i,j}$ determines how vehicle i responds to the motion of vehicle j (see Fig. 3). In practice, the acceleration u_i is bounded by an upper bound $a_{\max,i} > 0$ and a lower bound $a_{\min,i} < 0$, where the magnitude of $a_{\min,i}$ denotes the maximum deceleration. Thus, we impose the constraint $a_{\min,i} \le u_i(t) \le a_{\max,i}$ for all $t \ge 0$.

For selective use of the information received from vehicle j, we propose a strategy

$$\gamma_{i,j} = \begin{cases} 1, & \text{if } f_{i,j}(s_j, s_i, v_j, v_i) < 0, \\ 0, & \text{otherwise}. \end{cases} \tag{3}$$

Note that $\gamma_{i,i-1} = 1$ always holds since CAVs shall always respond to the motion of the vehicle immediately ahead for safety. The logic behind strategy (3) is stated as follows. When the motion of vehicle j leads to $f_{i,j} < 0$, it implies that either the distance between vehicles i and j is smaller than the desired distance or the speed of vehicle j is smaller than that of vehicle i. In this case, CACC shall respond for improving vehicle safety. In the opposite case when $f_{i,j} \ge 0$, vehicle i shall not respond to the motion of vehicle j to prevent the collision mentioned in Fig. 1.

In general, the function $f_{i,j}$ in (2) can be designed in any form. Here, we use

$$f_{i,j}(s_j, s_i, v_j, v_i) = \alpha_{i,j}(V_i(h_{i,j}) - v_i) + \beta_{i,j}(U_i(v_j) - v_i), \tag{4}$$

where the positive gains $\alpha_{i,j}$ and $\beta_{i,j}$ are used to regulate the inter-vehicle distances and the relative velocity between vehicles i and j, respectively. The quantity

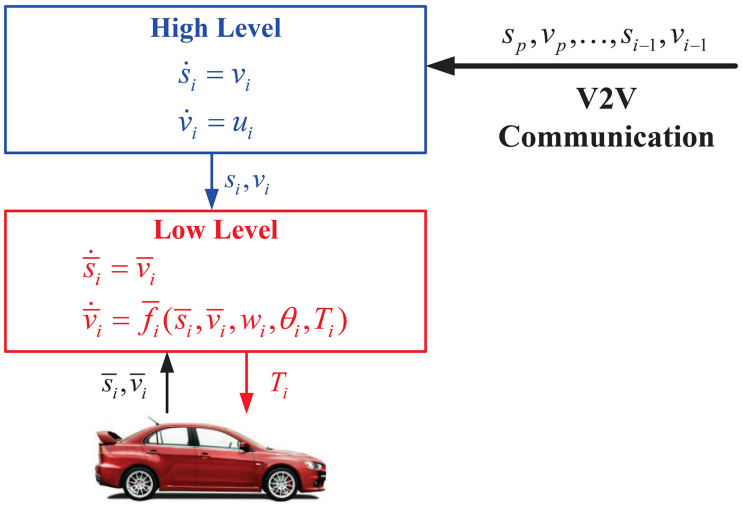

Fig. 4 *Hierarchical framework for CACC design [15]. At the high level, the acceleration u_i is designed to determine the desired position s_i and the desired velocity v_i by incorporating the motion data received from vehicles $j = p, \ldots, i-1$. At the low level, a physics-based dynamic model is considered to design the actuation input T_i (e.g. engine torque and brake) such that the real position $\bar{s}_i$ and real velocity $\bar{v}_i$ can track their desired values s_i and v_i, respectively. The external disturbance w_i is composed of headwind speed and road angle, while θ_i is composed of vehicle parameters (e.g. vehicle mass, aerodynamic drag coefficient etc.). A specific physics-based vehicle dynamic model is given in Section 7.2*

$$h_{i,j} = \frac{s_j - s_i - \sum_{\ell=j}^{i-1} l_\ell}{i-j} \tag{5}$$

represents the average inter-vehicle distance between vehicles i and j (see Fig. 3). Here, the quantity i–j represents the number of vehicles between vehicles i and j. In a vehicle chain that includes non-broadcasting vehicles, the value of i–j can be obtained by applying the link-length estimator proposed in [23]. The range policy $V_i(h)$ in (4) determines the desired velocity as a function of the inter-vehicle distance h in the form

$$V_i(h) = \begin{cases} 0, & \text{if } h \le h_{\mathrm{st},i}, \\ \dfrac{v_{\max}(h - h_{\mathrm{st},i})}{h_{\mathrm{go},i} - h_{\mathrm{st},i}}, & \text{if } h_{\mathrm{st},i} < h < h_{\mathrm{go},i}, \\ v_{\max}, & \text{if } h \ge h_{\mathrm{go},i}, \end{cases} \tag{6}$$

where $h_{\mathrm{st},i}$, $h_{\mathrm{go},i}$, and $v_{\max}$ are all positive constants. This implies that the vehicle tends to stop for small distances $h \le h_{\mathrm{st},i}$ while it aims to maintain the preset maximum speed $v_{\max}$ for large distances $h \ge h_{\mathrm{go},i}$. In the middle range $h_{\mathrm{st},i} < h < h_{\mathrm{go},i}$, the desired velocity increases when the distance h increases. One can use large values for $h_{\mathrm{st},i}$ and $h_{\mathrm{go},i}$ to enhance safety, but it also increases inter-vehicle distances and hence reduces traffic capacities. For different vehicles, the parameters in (6) may be different. In case that the vehicles ahead may over speed, we apply the saturation function

$$U_i(v) = \begin{cases} v, & \text{if } v \le v_{\max}, \\ v_{\max}, & \text{otherwise}, \end{cases} \tag{7}$$

for the desired velocity. Note that the preset maximum speed $v_{\max}$ is used to constrain the speed at steady state. The transient speed may temporarily exceed $v_{\max}$ due to the possible overshoots. When vehicles drive forward, the deceleration is generated by brakes, which cannot lead to negative speed.

Combining (1), (2), and (4) leads to the closed-loop longitudinal dynamics of CAVs

$$\begin{aligned} \dot{s}_i(t) &= v_i(t), \\ \dot{v}_i(t) &= \sum_{j=p}^{i-1} \gamma_{i,j}\big[\alpha_{i,j}(V_i(h_{i,j}(t-\sigma_i)) - v_i(t-\sigma_i)) \\ &\quad + \beta_{i,j}\big(U_i(v_j(t-\sigma_i)) - v_i(t-\sigma_i)\big)\big]. \end{aligned} \tag{8}$$

Based on the model (8), we investigate the design of control gains $\alpha_{i,j}, \beta_{i,j}$ to improve the safety and the comfort of CAVs in mixed traffic that include human-driven vehicles which may or may not broadcast information.

3 Data-driven optimisation of control gains

In this section, we study the data-driven optimisation of control gains. A fundamental requirement for safety is that CACC guarantees the internal stability of CAVs. The stability analyses of CACC in mixed traffic presented in [14–19] were based on non-selective strategies and hence they cannot be applied when the information provided by V2V communication is selectively used. Thus, we begin by deriving a condition that guarantees the internal stability of CAVs that exploit selective CACC.

3.1 Internal stability

The motion of a vehicle chain is said to be in equilibrium when all vehicles move at the same constant speed v^*. Note that the equilibrium distances are also constant but they may be different (i.e. $h^*_{j,j-1} \ne h^*_{k,k-1}$ for $j \ne k$) if vehicles use different range policies. Let s^*_j and v^*_j be the equilibrium positions and the equilibrium velocities of vehicles $j = p, \ldots, i$. Then, we have

$$s^*_{j-1} - s^*_j - l_{j-1} = h^*_{j,j-1}, \quad v^*_j = v^*, \tag{9}$$

for all j–s. It follows that the equilibrium average inter-vehicle distance between vehicles i and j is given by

$$h^*_{i,j} = \frac{s^*_j - s^*_i - \sum_{\ell=j}^{i-1} l_\ell}{i-j}, \tag{10}$$

cf. (5). Also, the motion of vehicle i is said to be internally stable if its state s_i, v_i approaches its equilibrium s^*_i, v^*_i in the absence of disturbances from other vehicles.

In practice, the average distance $h_{i,j}$ and velocity v_j can be any positive values. However, the domain of our interest is

$$\begin{aligned} \mathscr{D}_h &= \{h_{i,j} : h_{st,i} < h_{i,j} < h_{go,i}\}, \\ \mathscr{D}_v &= \{v_j : 0 < v_j < v_{\max}\}, \end{aligned} \tag{11}$$

since only in this domain the desired velocity $V_i(h_{i,j})$ changes with the inter-vehicle distance $h_{i,j}$; cf. (6). Then, in the following

theorem, a condition is presented for choosing gains that ensure the internal stability of CAVs with selective CACC.

Theorem 1: Suppose that the average distances and velocities are in the domain (11). Then, the longitudinal dynamics of CAVs given in (8) is internally stable in the presence of switching connectivity topologies and varying gains if there exist positive definite matrices $\boldsymbol{P}, \boldsymbol{Q}, \boldsymbol{W}$ such that the matrix

$$\boldsymbol{\Xi} = \begin{bmatrix} \boldsymbol{\Xi}_{1,1} & \boldsymbol{\Xi}_{1,2} & -\boldsymbol{P}\left(\sum_{j=p}^{i-1} \boldsymbol{A}_{i,j}\right) \\ \boldsymbol{\Xi}_{1,2}^{\mathrm{T}} & \boldsymbol{\Xi}_{2,2} & \boldsymbol{0}_{2\times 2} \\ -\left(\sum_{j=p}^{i-1} \boldsymbol{A}_{i,j}\right)^{\mathrm{T}} \boldsymbol{P} & \boldsymbol{0}_{2\times 2} & -\boldsymbol{W} \end{bmatrix} \tag{12}$$

is negative definite, where $\boldsymbol{0}_{2\times 2}$ denotes the two-dimensional zero matrix and

$$\begin{aligned} \boldsymbol{\Xi}_{1,1} &= \frac{\left(\sum_{j=p}^{i} \boldsymbol{A}_{i,j}\right)^{\mathrm{T}} \boldsymbol{P} + \boldsymbol{P}\left(\sum_{j=p}^{i} \boldsymbol{A}_{i,j}\right) + \boldsymbol{Q}}{\sigma_i} + \boldsymbol{A}_{i,i}^{\mathrm{T}} \boldsymbol{W} \boldsymbol{A}_{i,i}, \\ \boldsymbol{\Xi}_{1,2} &= \boldsymbol{A}_{i,i}^{\mathrm{T}} \boldsymbol{W} \left(\sum_{j=p}^{i-1} \boldsymbol{A}_{i,j} \right), \\ \boldsymbol{\Xi}_{2,2} &= \frac{\sigma_i \left(\sum_{j=p}^{i-1} \boldsymbol{A}_{i,j}\right)^{\mathrm{T}} \boldsymbol{W} \left(\sum_{j=p}^{i-1} \boldsymbol{A}_{i,j}\right) - \boldsymbol{Q}}{\sigma_i}, \end{aligned} \tag{13}$$

with matrices given by

$$\begin{aligned} \boldsymbol{A}_{i,j} &= \begin{bmatrix} 0 & 0 \\ -\dfrac{\gamma_{i,j}\alpha_{i,j} v_{\max}}{(i-j)(h_{\mathrm{go},i} - h_{\mathrm{st},i})} & -\gamma_{i,j}(\alpha_{i,j} + \beta_{i,j}) \end{bmatrix}, \\ \boldsymbol{A}_{i,i} &= \begin{bmatrix} 0 & 1 \\ 0 & 0 \end{bmatrix}, \end{aligned} \tag{14}$$

where $j = p, \ldots, i-1$. The proof of Theorem 1 is given in Section 7.1. Since the connectivity topologies may vary, we consider the combinations of gains $\sum_{j=p}^{i-1} \gamma_{i,j}\alpha_{i,j}/(i-j)$ and $\sum_{j=p}^{i-1} \gamma_{i,j}(\alpha_{i,j} + \beta_{i,j})$ as variables when solving the linear matrix inequalities (LMIs) in Theorem 1; cf. (14). We solve the LMIs by applying the numerical solver YALMIP [24], leading to a region for choosing gains that ensure the internal stability. In real traffic when the motion of vehicles is not in equilibrium, satisfying Theorem 1 leads to stable car-following dynamics of CAVs. This is necessary for safety because unstable car-following dynamics may result in collisions. When the states are outside the domain (11), the longitudinal dynamics of CAVs is still determined by the controllers (2) and (4) with the range policy (6), but the internal stability may not be guaranteed. For example, if the CAV is a heavy-duty truck with lower maximum speed than the speed of vehicles ahead, the CAV will maintain its maximum speed but its distances from vehicles ahead keep increasing instead of reaching a constant equilibrium. The capabilities of acceleration and deceleration do not affect the internal stability if the control gains are chosen according to Theorem 1, however, lower maximum deceleration increases the risk of collisions and hence requires large values for $h_{\mathrm{st},i}$ and $h_{\mathrm{go},i}$ in the range policy (6) to enhance safety.

3.2 Data-driven optimisation

After the internal stability is guaranteed, another desired property is that CAVs are able to attenuate the disturbances arising from vehicles ahead. Due to the incorporation of human-driven vehicles of which the dynamics are unknown, disturbance attenuation of CAVs in mixed traffic cannot be ensured through analytical analysis. To address this problem, we apply a data-driven approach for online optimisation of control gains. In particular, we first choose the gains $\alpha_{i,i-1}$ and $\beta_{i,i-1}$ within the stability region presented in [14], which enables CAV i to attenuate the perturbations arising from vehicle $i-1$ when the motion data received from all other vehicles $j < i-1$ are not utilised. Then, the other gains $\alpha_{i,j}$ and $\beta_{i,j}$ $(j < i-1)$ are optimised by using the historical data of broadcasting vehicles. According to the UMTRI Safety Pilot Project [25], V2V communication provides information to every $\delta t = 0.1$ s. To make the subsequent expressions more compact, we define vectors

$$\begin{aligned} \overline{\boldsymbol{u}}_i(t_k) &= [u_i(t_{k-\Delta}), \ldots, u_i(t_k)], \\ \overline{\boldsymbol{V}}_i(t_k) &= [V_i(h_{i,i-1}(t_{k-\Delta})), \ldots, V_i(h_{i,i-1}(t_k))], \\ \overline{\boldsymbol{v}}_i(t_k) &= [v_i(t_{k-\Delta}), \ldots, v_i(t_k)], \end{aligned} \tag{15}$$

where $t_k = k \cdot \delta t$ for $k = 0, 1, 2, \ldots$, and the symbol Δ denotes the amount of historical data stored in the memory. For optimisation, we consider the following cost function: (see (16)) where c_1 and c_2 are positive constants. This cost function is designed by considering the trade-off between comfort, safety, and traffic efficiency. The first term is used to avoid large accelerations and decelerations for improving passengers' comfort. The second term is used to make the velocity track the desired distance-dependent velocity determined by the range policy (6), in order to maintain the desired distance from the vehicle immediately ahead. The third term is used to attenuate the velocity perturbations, which has potential for improving traffic efficiency. In practice, safety shall be the most critical, while comfort may be more important than traffic efficiency. Thus, we choose the weights such that $c_1 > 1 > c_2$, where 1 is indeed the gain of the first term. Note that the cost function (16) depends on the gains $\alpha_{i,j}$ and $\beta_{i,j}$ through the dynamics (8). The ∞-norm used in the cost function (16) is defined by

$$\| \overline{\boldsymbol{u}}_i(t_k) \|_\infty = \max_{\ell = 0, \ldots, \Delta} |u_i(t_{k-\ell})|, \tag{17}$$

which is used to evaluate the peak value. The expectation operator

$$\mathbb{E}[\overline{\boldsymbol{v}}_i(t_k)] = \frac{1}{\Delta + 1} \sum_{\ell=0}^{\Delta} v_i(t_{k-\ell}) \tag{18}$$

is used to calculate the average of the data in memory.

To find the optimal gains that minimise the cost (16), we apply a data-driven approach by utilising the historical motion data of other vehicles received from V2V communication. The process for implementing the data-driven optimisation is summarised in the flow chart shown in Fig. 5. When V2V communication receives information from vehicles ahead, it will store the data in the memory and increment the data length; cf. (15). The optimisation of gains is triggered when the data length Δ reaches the given threshold $\overline{\Delta}$. Since a small amount of data is insufficient for finding appropriate results while a large amount of data increases computation time, the threshold $\overline{\Delta}$ shall be chosen by considering the trade-off between the robustness and the real-time performance. To find the appropriate values for $\overline{\Delta}$, we have conducted a large number of simulations. Based on our observation, the appropriate values of $\overline{\Delta}$ are between 80 and 200, which corresponds to window size between 8 and 20 s.

In practice, the motion of closer vehicles shall have more impacts on the motion of CAVs. Accordingly, we choose $\alpha_{i,j} > \alpha_{i,k}$ and $\beta_{i,j} > \beta_{i,k}$ for any $j > k$; see Fig. 3. One crucial step for implementing the data-driven approach is to determine the ranges for sampling gains $\alpha_{i,j}$ and $\beta_{i,j}$ such that the internal stability is always ensured. In practice, we first select $\alpha_{i,i-1}$ and $\beta_{i,i-1}$ that ensure the internal stability and also enable CAV i to attenuate the perturbations arising from vehicle $i-1$ when CAV i does not utilise the information received from vehicles $j < i-1$. Then, we

$$J = \| \overline{\boldsymbol{u}}_i(t_k) \|_\infty + c_1 \| \overline{\boldsymbol{V}}_i(t_k) - \overline{\boldsymbol{v}}_i(t_k) \|_\infty + c_2 \| \overline{\boldsymbol{v}}_i(t_k) - \mathbb{E}[\overline{\boldsymbol{v}}_i(t_k)] \|_\infty, \tag{16}$$

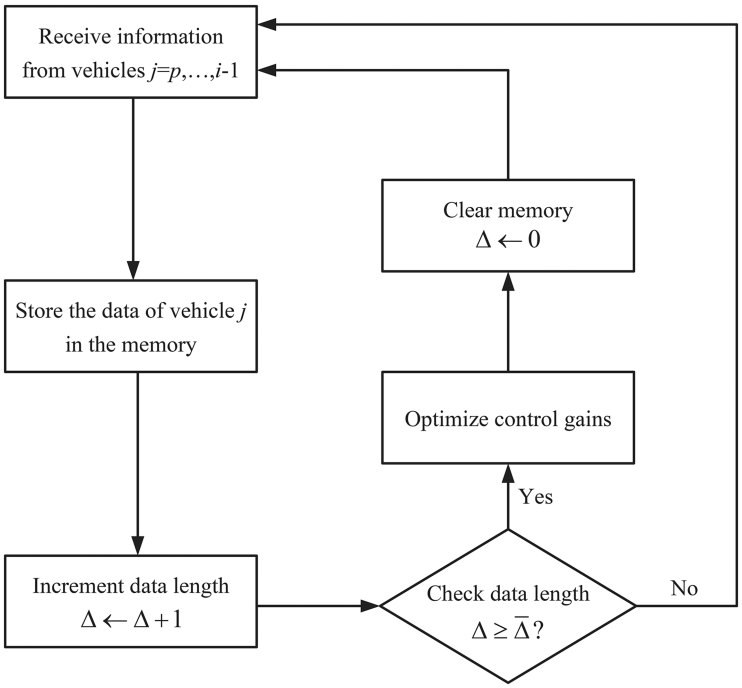

Fig. 5 *Process flow for data-driven optimisation of CACC gains*

propose an approach to determine the ranges for sampling the other gains. Specifically, we create a rectangle which takes $(\alpha_{i,i-1}+\beta_{i,i-1}, \alpha_{i,i-1})$ as the lower left vertex and expands the rectangle by keeping the ratio between length and height as 2 to 1 until the rectangle reaches the boundary of internal stability region. Suppose that the height of the largest rectangle is $H_{\max,i}$. Then, the values of $\alpha_{i,j}$ and $\beta_{i,j}$ can be selected between $2^{-(i-j)}H_{\max,i}$ and $2^{-(i-j-1)}H_{\max,i}$ for $j < i-1$. Since $\lim_{p\to-\infty}\sum_{j=p}^{i-2}2^{-(i-j-1)}=1$, it follows that the combinations of gains $\sum_{j=p}^{i-1}\gamma_{i,j}\alpha_{i,j}/(i-j)$ and $\sum_{j=p}^{i-1}\gamma_{i,j}(\alpha_{i,j}+\beta_{i,j})$ are always within the rectangle such that the internal stability of CAVs with selective CACC is guaranteed.

For data-driven optimisation of gains, we randomly sample N sets of gains $\{\alpha_{i,p}, \beta_{i,p}, \ldots, \alpha_{i,i-2}, \beta_{i,i-2}\}$ in the corresponding ranges based on the uniform distribution. Then, by using the historical motion data of broadcasting vehicles stored in the memory, we simulate the dynamics (8) with the sampled gains, which yields the cost for each sampled set of gains. Finally, we select the set of gains associated with the minimum cost and keep using them until the next update. The computation time for optimisation is determined by the threshold of data length $\overline{\Delta}$ and the number of samples N. To achieve real-time performance, the value of N shall decrease when the value of $\overline{\Delta}$ increases. Note that significant changes in gains may lead to large jerks through the longitudinal dynamics (8), which may cause passengers' discomfort. Thus, at each period we bound the variation of gains to one-tenth of corresponding ranges.

4 Numerical simulations

In this section, we evaluate the performance of selective CACC by using numerical simulations. To enhance the fidelity of simulations, we consider the physics-based vehicle dynamics for CAVs, which include aerodynamic drags and rolling resistance; for details see Section 7.2. Then, we apply the selective CACC as a high-level controller through the hierarchical control architecture shown in Fig. 4, where a low-level controller regulates the vehicle to track the desired motion generated by selective CACC. For CAV i, the symbols s_i and v_i obtained from CACC (8) are treated as the desired states, and we use symbols $\bar{s}_i$ and $\bar{v}_i$ for the real position and the real velocity which are obtained by solving the physics-based vehicle model with the low-level controller. For the motion of human-driven vehicles, we first apply car-following models to demonstrate the response of selective CACC in extreme cases. Then, we also test the selective CACC by using the experimental data of human-driven vehicles.

4.1 Simulation using car-following models

Here, we conduct simulations by considering the eight-vehicle chain displayed in Fig. 6, which is composed of CAVs (e.g. vehicles 4 and 7), human-driven vehicles that broadcast information (e.g. vehicles 0, 2, and 5), and human-driven vehicles that do not broadcast information (e.g. vehicles 1, 3, and 6). Human-driven vehicles only respond to the motion of the vehicle immediately ahead, while CAVs respond to the vehicle immediately ahead and they can also access the motion data of distant broadcasting vehicles through V2V communication. For simulating the dynamics of human-driven vehicles, the optimal velocity model (OVM) and the intelligent driver model (IDM) are widely used [26]. OVM is indeed given by (8) but setting $\gamma_{i,i-1}=1$ while $\gamma_{i,j}=0$ for all $j\neq i-1$. IDM is in the form [27]

$$\begin{aligned}\dot{s}_j(t) &= v_j(t),\\ \dot{v}_j(t) &= a_{\max,j}\left[1-\left(\frac{v_j(t-\sigma_j)}{v_{\max,j}}\right)^4\right.\\ &\quad\left.-\left(\frac{g(v_j(t-\sigma_j), v_{j-1}(t-\sigma_j))}{h_{j,j-1}(t-\sigma_j)}\right)^2\right],\end{aligned} \tag{19}$$

where

$$g(v_j, v_{j-1}) = h_{\mathrm{st},j} + v_j T_j + \frac{v_j(v_j - v_{j-1})}{2\sqrt{|a_{\max,j}\cdot a_{\min,j}|}}. \tag{20}$$

Here, σ_j represents the response time of the human driver, T_j is the desired time gap, and $a_{\max,j}$ and $a_{\min,j}$ denote the maximum acceleration and the maximum deceleration, respectively.

We assume that the leading vehicle 0 has length $l_0 = 4.8$ m and its speed profile is given by the experimental data collected through the UMTRI Safety Pilot Project [25]. Considering the heterogeneity in real traffic, we use different models and different parameters for different vehicles, as listed in Table 2. Although $a_{\max,k}$ and $a_{\min,k}$ are not explicitly expressed in OVM and CACC (8), we use them to constrain the acceleration inputs such that neither acceleration nor deceleration will exceed the limits. Moreover, when the speed becomes zero while CACC still requests

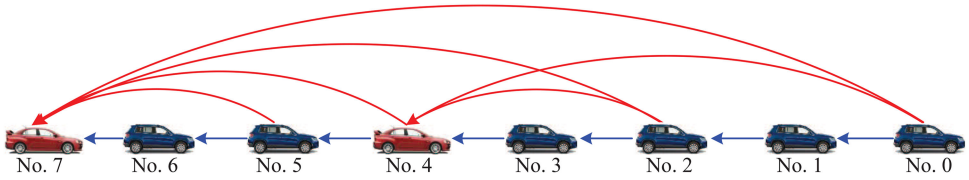

Fig. 6 *An 8-vehicle chain which is composed of CAVs (e.g. vehicles 4 and 7), human-driven vehicles that broadcast information (e.g. vehicles 0, 2, and 5), and human-driven vehicles that do not broadcast information (e.g. vehicles 1, 3, and 6)*

Table 2 Models and parameters for vehicles 1–7 in the vehicle chain shown in Fig. 6

Vehicle k	1	2	3	4	5	6	7
Model	OVM	IDM	OVM	CACC	IDM	OVM	CACC
l_k, m	4.3	4.6	5.5	4	4.5	3.9	4.2
σ_k, s	0.5	0.6	0.7	0.2	0.5	0.6	0.2
$\alpha_{k,k-1}$, s^{-1}	0.6	N/A	0.5	1	N/A	2.5	1
$\beta_{k,k-1}$, s^{-1}	0.7	N/A	0.5	1.5	N/A	1.5	1
$h_{\mathrm{st},k}$, m	3	2	2	3	3	3	5
$h_{\mathrm{go},k}$, m	30	N/A	31	33	N/A	32	35
T_k, s	N/A	1	N/A	N/A	1.2	N/A	N/A
$v_{\max,k}$, m/s	30	30	30	30	30	30	30
$a_{\max,k}$, m/s^2	2.5	2.5	2.5	2.5	2.5	2.5	2.5
$a_{\min,k}$, m/s^2	−2	−2	−2	−2	−2	−2	−2

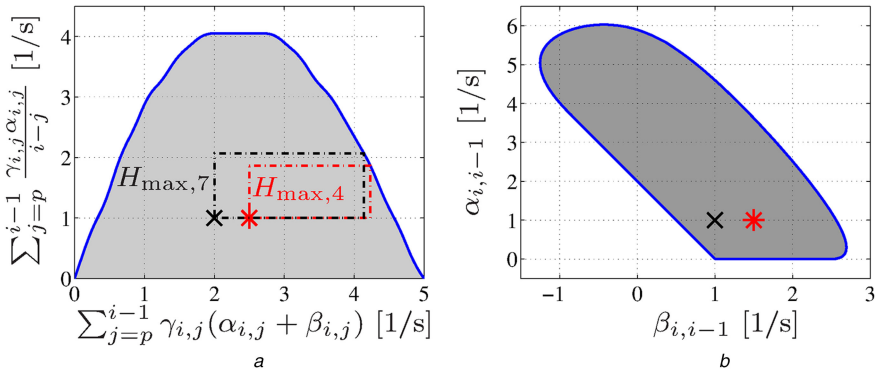

Fig. 7 *Stability regions for choosing control gains*

(a) The shaded region highlights the combinations of control gains that ensure the internal stability of CAVs, which is obtained according to Theorem 1 with range policy parameters given in Table 2. The domains enclosed by the dashed-dotted rectangles highlight the regions for sampling gains for vehicles 4 and 7, where the red star and black cross are determined by the chosen $(\alpha_{4,3}, \beta_{4,3})$ and $(\alpha_{7,6}, \beta_{7,6})$,

(b) The shaded domain is constructed according to the calculation presented in [14], which highlights the gains $\alpha_{i,i-1}$ and $\beta_{i,i-1}$ that enable CAVs to attenuate the disturbances arising from the vehicle immediately ahead when they do not utilise the information received from distant vehicles. For CAVs 4 and 7, the chosen gains $(\alpha_{4,3}, \beta_{4,3})$ and $(\alpha_{7,6}, \beta_{7,6})$ are marked by the red star and black cross, respectively

deceleration, we set the deceleration to be zero to avoid negative speed, since in practice brakes cannot lead to negative speed. In the simulation, when vehicle k collides with vehicle $k-1$, we freeze the position of vehicle k and also set its velocity and acceleration to be zeros.

Applying the parameters σ_k, $h_{\mathrm{st},k}$, $h_{\mathrm{go},k}$, and $v_{\max,k}$ ($k = 4$ and 7) given in Table 2 to Theorem 1 yields the region for selecting gains that guarantee the internal stability of CAVs, as shown by the shaded region in Fig. 7*a* (best viewed in colour online). In Fig. 7*b*, the shaded region marks the gains $\alpha_{i,i-1}$ and $\beta_{i,i-1}$ that enable CAVs to attenuate the perturbations arising from the vehicle immediately ahead when CACC does not utilise the information received from distant vehicles. In particular, for CAVs 4 and 7, we use the gains as marked by the red star and the black cross, respectively. Accordingly, in Fig. 7*a*, we obtain the corresponding ranges for sampling other gains as enclosed by the dashed-dotted rectangles. The control gains along the long-range links are randomly initialised within their corresponding ranges, and then they are updated through the data-driven optimisation presented in Section 3. For data-driven optimisation, we set $c_1 = 1.5$ and $c_2 = 0.5$ in the cost function (16), choose $\bar{\Delta} = 100$ for the threshold of data length, and sample $N = 100$ sets of gains. For this setup, the update of gains can be completed in 0.1 s.

To evaluate the performance of selective CACC, we consider two scenarios with two cases being compared for each scenario, as summarised in Table 3. First, we consider case I in Scenario I. The corresponding results are displayed in Fig. 8. In particular, Fig. 8*a* shows the inter-vehicle distances, where the zoomed-in panel highlights the moment when vehicle 0 makes a sharp brake. For CAVs 4 and 7, we use their real states such that $\bar{h}_{4,3} = s_3 - l_3 - \bar{s}_4$, $\bar{h}_{5,4} = \bar{s}_4 - l_4 - s_5$, and $\bar{h}_{7,6} = s_6 - l_6 - \bar{s}_7$. One can observe that the distances of vehicles 1–4 from the vehicles immediately ahead become zeros, implying that the sharp brake of vehicle 0 leads to a chain collision of vehicles 1–4. Fig. 8*b* shows the velocity of each vehicle, where the zoomed-in panel highlights the velocity of each vehicle when vehicle 0 sharply brakes. Fig. 8*c* shows that the acceleration requests of CAVs 4 and 7 never exceed their limits marked by dashed-dotted lines. Fig. 8*d* shows that the real state $\bar{s}_i, \bar{v}_i$ tracks the desired state s_i, v_i with small errors. The peak error between s_4 and $\bar{s}_4$ occurs when vehicle 4 collides with vehicle 3. To show multiple switch coefficients in one figure without overlaps, we add biases 2, 4, 6 to $\gamma_{7,4}$, $\gamma_{7,2}$, and $\gamma_{7,0}$, respectively; cf. (3). Then,

Table 3 Scenarios and cases for evaluating the performance of selective CACC

scenario I	vehicle 0 makes a sharp brake at $t = 180$ s with constant deceleration 2 m/s^2 until it stops
case I	vehicle 4 exploits ACC while vehicle 7 exploits selective CACC
case II	both vehicles 4 and 7 exploit selective CACC
scenario II	vehicle 1 makes a sharp brake at $t = 180$ s with constant deceleration 2 m/s^2 until it stops, while vehicle 0 maintains its speed profile
case I	vehicle 4 exploits non-selective CACC while vehicle 7 exploits selective CACC
case II	both vehicles 4 and 7 exploit selective CACC

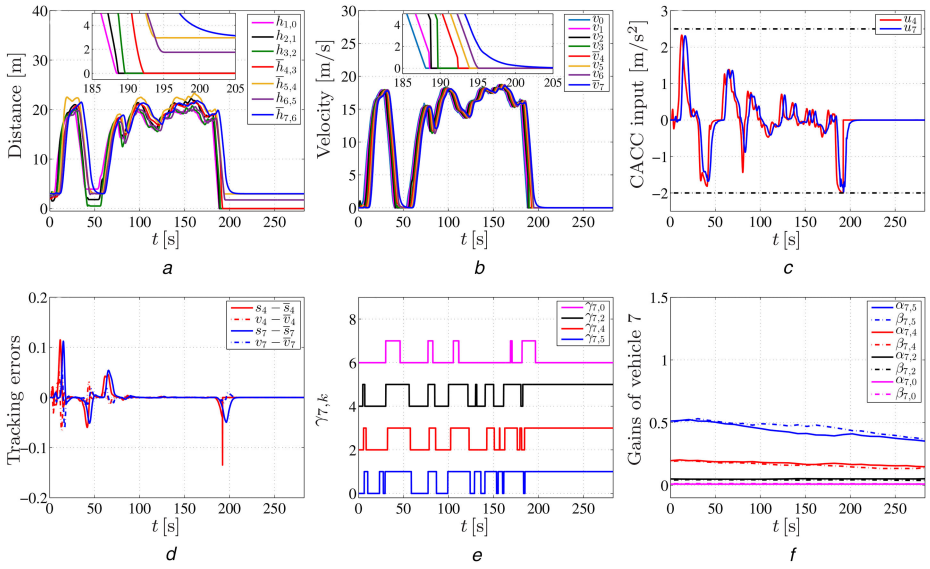

Fig. 8 *Simulation for case I in scenario I described in Table 3*

(a) Inter-vehicle distances of vehicles 1–7, where zero distance indicates the collision with the vehicle immediately ahead. The zoomed-in panel highlights the moment when vehicle 0 makes a sharp brake. Here, $\overline{h}_{4,3} = s_3 - l_3 - \overline{s}_4$, $\overline{h}_{5,4} = \overline{s}_4 - l_4 - s_5$, and $\overline{h}_{7,6} = s_6 - l_6 - \overline{s}_7$, where $\overline{s}_4$ and $\overline{s}_7$ denote the real positions of CAVs 4 and 7 that are obtained by solving the physics-based dynamic model,

(b) Velocities of vehicles 0–7,

(c) The acceleration inputs for vehicles 4 and 7, where the dashed-dotted lines represent the upper and lower bounds of accelerations,

(d) Errors between desired states s_i, v_i and real states $\overline{s}_i$, $\overline{v}_i$ of CAVs 4 and 7,

(e) Switch coefficients of vehicle 7. To show multiple switch coefficients in one figure without overlaps, we add biases 2, 4, and 6 to $\gamma_{7,4}$, $\gamma_{7,2}$, and $\gamma_{7,0}$, respectively. The low value of $\gamma_{7,j}$ indicates that the information of vehicle j is not utilised by vehicle 7, while the high value of $\gamma_{7,j}$ indicates that vehicle 7 utilises the information of vehicle j; cf. (3),

(f) Evolution of control gains of vehicle 7 that are determined by the data-driven optimisation

the switch coefficients of vehicle 7 are shown in Fig. 8*e*. Fig. 8*f* shows that the evolution of gains is mild such that the acceleration varies smoothly during the update of gains; see the blue curve in Fig. 8*c*.

Then, we consider case II in scenario I stated in Table 3. The corresponding results are summarised in Fig. 9 (best viewed in colour online). In particular, comparing $\overline{h}_{4,3}$ (red curve) in the zoomed-in panels of Figs. 8*a* and 9*a*, one can observe that selective CACC makes vehicle 4 avoid the collision by incorporating the motion data of distant vehicles received from V2V communication. Fig. 9*b* shows the velocities of vehicles 0–7. The acceleration inputs and the tracking errors of CAVs 4 and 7 are shown in Figs. 9*c* and *d*, respectively. In particular, the small steady error between s_4 and $\overline{s}_4$ at the end occurs since vehicle 4 stops in front of the desired position and cannot drive backwards. The switch coefficients and the evolution of gains of vehicle 7 are shown in Fig. 9*e* and *f* while those of vehicle 4 are shown in Figs. 9*g* and *h*. Note that we add a bias 2 to $\gamma_{4,0}$ in order to display $\gamma_{4,2}$ and $\gamma_{4,0}$ in the same figure without overlaps.

Now we consider scenario II described in Table 3 and compare the performance of non-selective CACC and that of selective CACC. We begin with case I such that vehicle 4 always utilise the motion data of vehicles 0 and 2. The corresponding coefficients are set to be $\alpha_{4,2} = 0.6$ s^{-1}, $\beta_{4,2} = 0.9$ s^{-1}, $\alpha_{4,0} = 0.14$ s^{-1}, and $\beta_{4,0} = 0.2$ s^{-1}. The simulation results are shown in Fig. 10 (best viewed in colour online). In particular, the zoomed-in panel in Fig. 10*a* shows that non-selective CACC causes a collision of vehicle 4 (red curve). This collision occurs because the motion of vehicle 0 leads to acceleration of vehicle 4 through the non-selective CACC.

Then, we consider case II in scenario II described in Table 3. The simulation results are displayed in Fig. 11 (best viewed in colour online). Comparing the distance between vehicles 3 and 4 (red curve) in the zoomed-in panels of Figs. 10*a* and 11*a*, one can observe that selective CACC makes vehicle 4 avoid the collision caused by non-selective CACC. The switch coefficient $\gamma_{4,0}$ (red curve) in Fig. 11*g* indicates that the CAV 4 ignores the motion of vehicle 0 immediately after vehicle 1 makes a sharp brake such that the motion of vehicle 0 does not lead to an acceleration of vehicle 4. This contributes to the avoidance of the collision caused by non-selective CACC.

For the simulation results above, CAV 4 demonstrates the advantages of selective CACC for enhancing safety, while CAV 7 is used to show that the proposed selective CACC can be applied when the number of vehicles increases and when the complexity of connectivity topology increases.

4.2 Simulation using experimental data

Here, we consider the five-vehicle chain as shown in Fig. 12 where vehicle 4 is a CAV that monitors the motion of human-driven vehicles 0–3 through V2V communication. The motion of human-driven vehicles 0–3 are given by the data collected through an on-road experiment along a 4.5 km long section of Mast road near Dexter, Michigan, USA; see [28]. Then, we consider the physics-based dynamics given in Appendix B for CAV 4 and apply the selective CACC through the hierarchical control architecture shown in Fig. 4. The corresponding results are shown in Fig. 13 (best viewed in colour online). In particular, Fig. 13*a* shows that the selective CACC attenuates the perturbations caused by human-

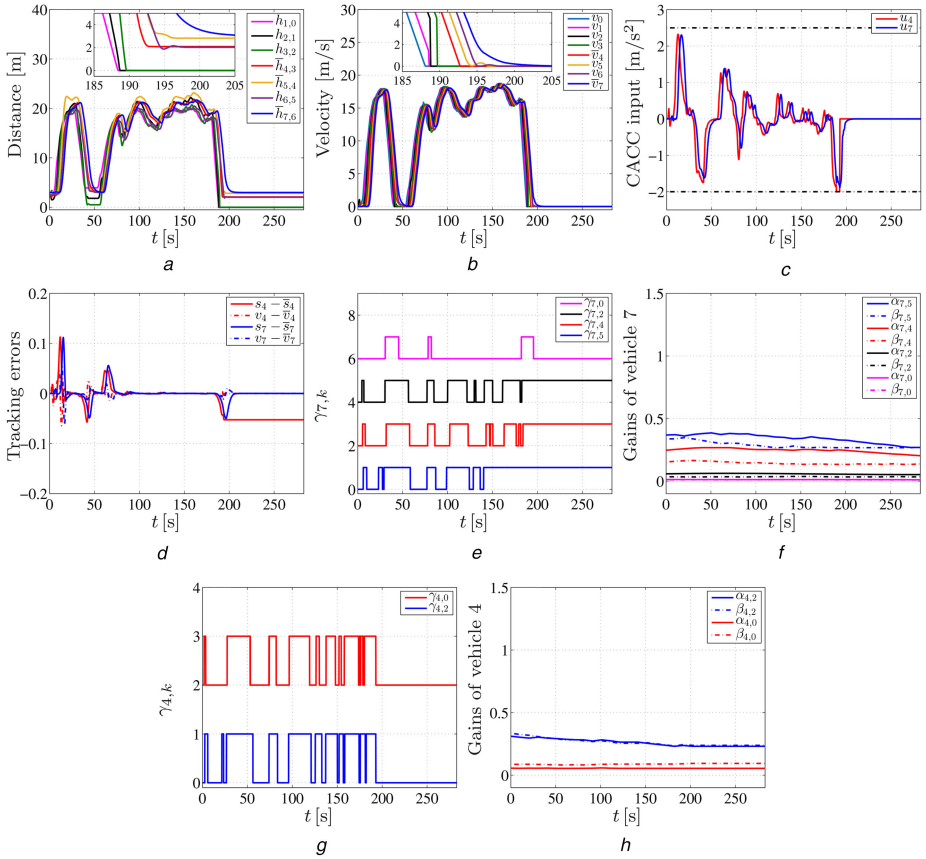

Fig. 9 *Simulation for case II in scenario I described in Table 3. Notations are the same as used in Fig. 8. In particular, incorporating the motion data of distant vehicles in CACC makes vehicle 4 avoid the collision; compare Figs. 8a and 9a. In (g), a bias 2 is added to $\gamma_{4,0}$ such that the switch coefficients $\gamma_{4,0}$ and $\gamma_{4,2}$ can be displayed in one figure without overlaps. The low value of $\gamma_{4,j}$ indicates that the information of vehicle j is not utilised by vehicle 4, while the high value of $\gamma_{4,j}$ indicates that vehicle 4 utilises the information of vehicle j; cf. (3)*

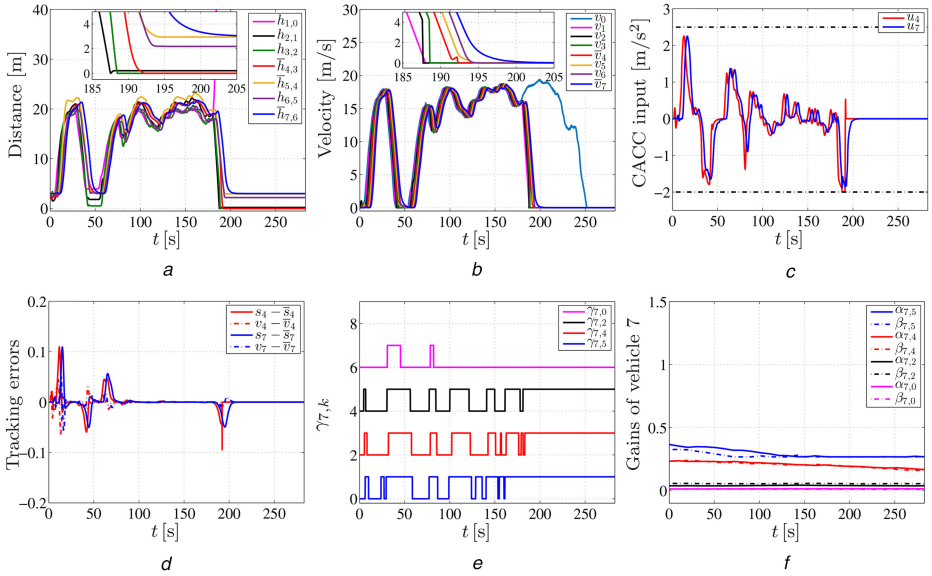

Fig. 10 *Simulation for case I in scenario II described in Table 3. Notations are the same as used in Fig. 8*

driven vehicles; compare the red curve and other curves. The noises in Figs. 13*c* and *d* arise due to the measurement noises in the collected experimental data. The switch coefficients and the evolution of control gains are displayed in Figs. 13*e* and *f*, respectively.

5 Conclusions

In this study, we investigated the design of CACC that selectively incorporated the motion data of other vehicles received through V2V communication. A condition was derived for choosing control gains that guaranteed the internal stability of selective CACC in the presence of switching connectivity topologies and varying gains. A data-driven approach was applied for online optimisation of control gains without requiring the knowledge about the dynamics of other vehicles, which was particularly useful in mixed traffic comprised of human-driven vehicles. Numerical simulations demonstrated the advantages of the proposed selective CACC in improving vehicle safety and reducing perturbations.

In future, we will improve the safety of selective CACC by explicitly including safety distance constraints. Moreover, the

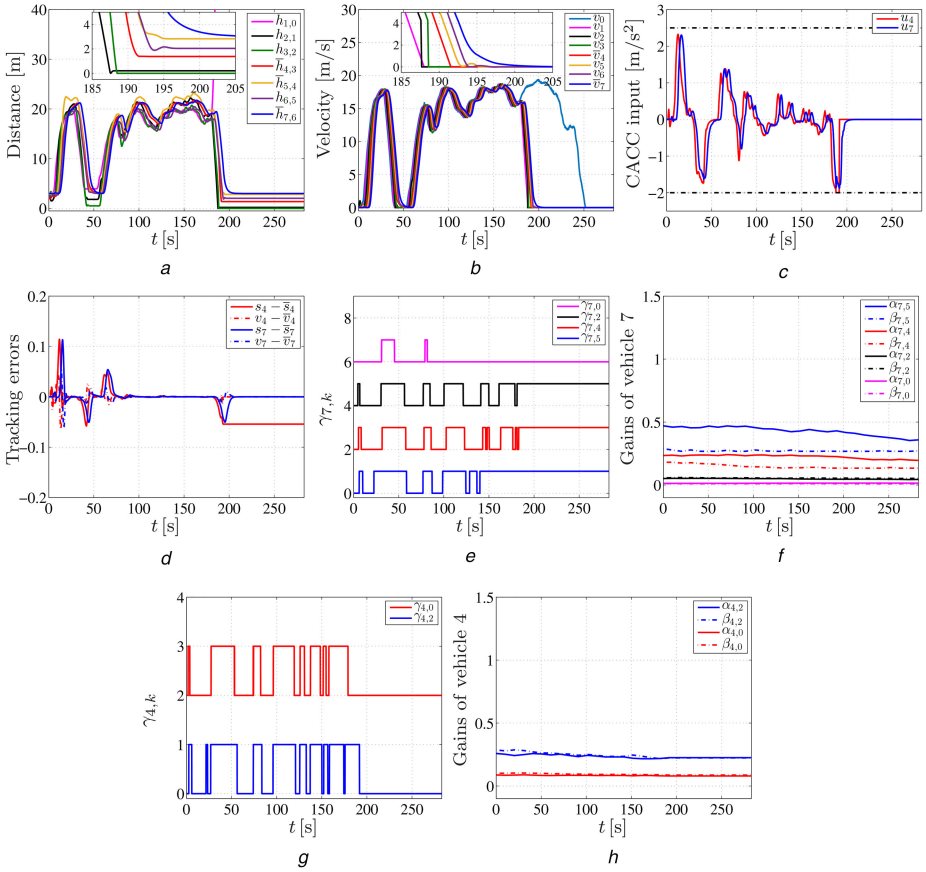

Fig. 11 *Simulation for case II in scenario II described in Table 3. Notations are the same as used in Fig. 9. In particular, $\gamma_{4,0}$ in (g) indicates that the selective CACC of CAV 4 discards the motion data of vehicle 0 immediately after vehicle 1 makes a sharp brake, which makes vehicle 4 avoid the collision; compare $\overline{h}_{4,3}$ (red curve) in the zoomed-in panels of Figs. 10a and 11a*

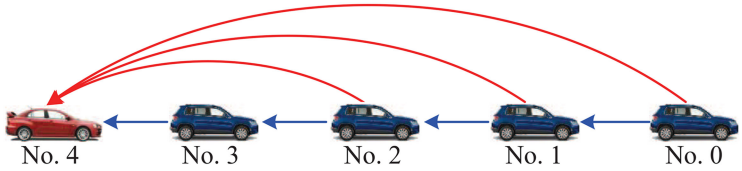

Fig. 12 *A 5-vehicle chain where vehicle 4 is a CAV that monitors the motion of human-driven vehicles 0–3 through V2V communication*

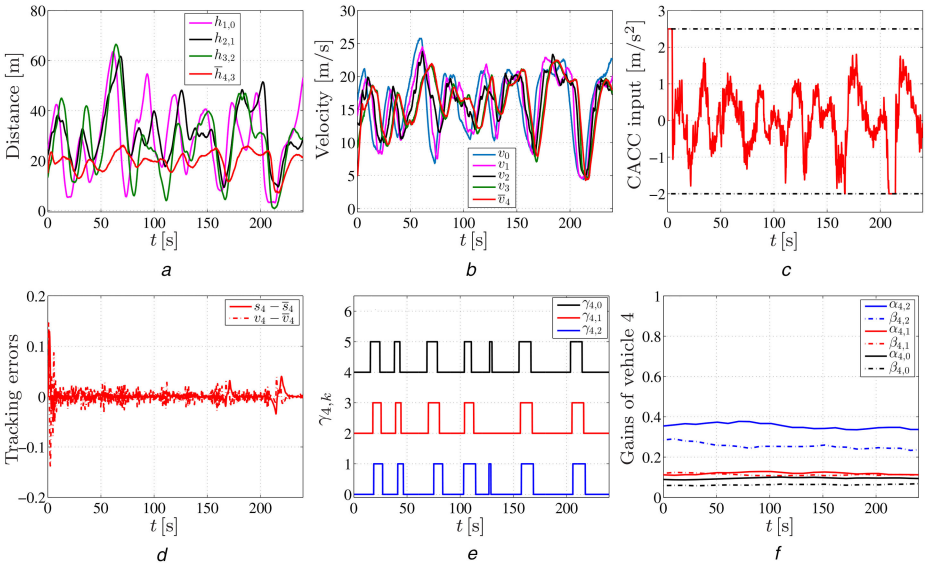

Fig. 13 *Application of selective CACC to vehicle 4 in the vehicle chain shown in Fig. 12. The motion of human-driven vehicles 0–3 is given by the data collected through on-road experiments. Notations are the same as used in Fig. 8. In particular, panel (a) demonstrates that selective CACC attenuates the perturbations caused by human-driven vehicles; compare the red curve and the curves of other colours*

optimisation of the selection strategies for efficient use of V2 V communication will also be investigated.

6 References

[1] Vahidi, A., Eskandarian, A.: 'Research advances in intelligent collision avoidance and adaptive cruise control', *IEEE Trans. Intell. Transp. Syst.*, 2003, **4**, (3), pp. 143–153

[2] Dar, K., Bakhouya, M., Gaber, J., *et al.*: 'Wireless communication technologies for ITS application', *IEEE Commun. Mag.*, 2010, **48**, (5), pp. 156–162

[3] Morgan, Y.L.: 'Notes on DSRC & WAVE standards suite: its architecture, design, and characteristics', *IEEE Commun. Surv. Tutor.*, 2010, **12**, (4), pp. 504–518

[4] Dey, K.C., Yan, L., Wang, X., *et al.*: 'A review of communication, driver characteristics, and controls aspects of cooperative adaptive cruise control', *IEEE Trans. Intell. Transp. Syst.*, 2016, **17**, (2), pp. 491–509

[5] Seiler, P., Pand, A., Hedrick, K.: 'Disturbance propagation in vehicle strings', *IEEE Trans. Autom. Control*, 2004, **49**, (10), pp. 1835–1842

[6] Zhao, Y., Minero, P., Gupta, V.: 'On disturbance propagation in leader-follower systems with limited leader information', *Automatica*, 2014, **50**, pp. 591–598

[7] Naus, G.J.L., Vugts, R.P.A., Ploeg, J., *et al.*: 'String-stable CACC design and experimental validation: a frequency-domain approach', *IEEE Trans. Veh. Technol.*, 2010, **59**, (9), pp. 4268–4279

[8] Ploeg, J., Shukla, D.P., van de Wouw, N., *et al.*: 'Controller synthesis for string stability of vehicle platoons', *IEEE Trans. Intell. Transp. Syst.*, 2014, **15**, (2), pp. 854–865

[9] Zheng, Y., Li, S.E., Wang, J., *et al.*: 'Stability and scalability of homogeneous vehicular platoon: study on the influence of information flow topologies', *IEEE Trans. Intell. Transp. Syst.*, 2016, **17**, (1), pp. 14–26

[10] Milanés, V., Shladover, S.E.: 'Modeling cooperative and autonomous adaptive cruise control dynamic response using experimental data', *Transp. Res. C*, 2014, **48**, pp. 285–300

[11] Robinson, T., Chan, E., Coelingh, E.: 'Operating platoons on public motorways: an introduction to the SARTRE platooning programme'. Proc. 17th World Congress on Intelligent Transport Systems, 2010, pp. 1–11

[12] Geiger, A., Lauer, M., Moosmann, F., *et al.*: 'Team AnnieWAY's entry to the 2011 grand cooperative driving challenge', *IEEE Trans. Intell. Transp. Syst.*, 2012, **13**, (3), pp. 1008–1017

[13] Alam, A., Mårtensson, J., Johansson, K.H.: 'Experimental evaluation of decentralized cooperative cruise control for heavy-duty vehicle platooning', *Control Eng. Pract.*, 2015, **38**, pp. 11–25

[14] Zhang, L., Orosz, G.: 'Motif-based design for connected vehicle systems in presence of heterogeneous connectivity structures and time delays', *IEEE Trans. Intell. Transp. Syst.*, 2016, **17**, (6), pp. 1638–1651

[15] Zhang, L., Sun, J., Orosz, G.: 'Hierarchical design of connected cruise control in the presence of information delays and uncertain vehicle dynamics', *IEEE Trans. Control Syst. Technol.*, 2018, **26**, (1), pp. 139–150

[16] Avedisov, S.S., Orosz, G.: 'Nonlinear network modes in cyclic systems with applications to connected vehicles', *J. Nonlinear Sci.*, 2015, **25**, (4), pp. 1015–1049

[17] Zhang, L., Orosz, G.: 'Consensus and disturbance attenuation in multi-agent chains with nonlinear control and time delays', *Int. J. Robust Nonlinear Control*, 2017, **27**, (5), pp. 781–803

[18] Qin, W.B., Gomez, M.M., Orosz, G.: 'Stability and frequency response under stochastic communication delays with applications to connected cruise control design', *IEEE Trans. Intell. Transp. Syst.*, 2017, **18**, (2), pp. 388–403

[19] Ge, J.I., Orosz, G.: 'Optimal control of connected vehicle systems with communication delay and driver reaction time', *IEEE Trans. Intell. Transp. Syst.*, 2017, **18**, (8), pp. 2056–2070

[20] Marino, R., Scalzi, S., Netto, M.: 'Nested PID steering control for lane keeping in autonomous vehicles', *Control Eng. Pract.*, 2011, **19**, (12), pp. 1459–1467

[21] Kenney, J.B.: 'Dedicated short-range communications (DSRC) standards in the United States', *Proc. IEEE*, 2011, **99**, pp. 1162–1182

[22] Bergenhem, C., Hedin, E., Skarin, D.: 'Vehicle-to-vehicle communication for a platooning system', *Procedia – Soc. Behav. Sci.*, 2012, **48**, pp. 1222–1233

[23] Zhang, L., Orosz, G.: 'Black-box modeling of connected vehicle networks'. Proc. American Control Conf., 2016, pp. 2421–2426

[24] Lofberg, J.: 'YALMIP: a toolbox for modeling and optimization in MATLAB'. IEEE Symp. on Computer Aided Control Systems Design, 2004, pp. 284–289

[25] Bezzina, D., Sayer, J.: 'Safety pilot model deployment: test conductor team report' (Report No. DOT HS 812 171), 2015

[26] Orosz, G., Wilson, R.E., Stépán, G.: 'Traffic jams: dynamics and control', *Philos. Trans. R. Soc. A*, 2010, **368**, (1928), pp. 4455–4479

[27] Kesting, A., Treiber, M., Helbing, D.: 'Enhanced intelligent driver model to access the impact of driving strategies on traffic capacity', *Philos. Trans. R. Soc. A*, 2010, **368**, (1928), pp. 4585–4605

[28] Zhang, L., Orosz, G.: 'Beyond-line-of-sight identification by using vehicle-to-vehicle communication', *IEEE Trans. Intell. Transp. Syst.*, 2018, **19**, (6), pp. 1962–1972

[29] Krstic, M.: '*Delay compensation for nonlinear, adaptive and PDE systems*' (Birkhäuser, New York, USA, 2009)

[30] Ulsoy, A.G., Peng, H., Çakmakci, M.: '*Automotive control systems*' (Cambridge University Press, 2012)

7 Appendix

7.1 Proof of theorem 1

We define the perturbations about equilibrium (9) as

$$\boldsymbol{x}_j = \begin{bmatrix} \tilde{s}_j \\ \tilde{v}_j \end{bmatrix} = \begin{bmatrix} s_j - s_j^* \\ v_j - v^* \end{bmatrix}, \tag{21}$$

for all $j - s$. When vehicles $p, \ldots, i-1$ are in the equilibrium and the states are in the domain (11), we substitute equilibrium (9) into the model (8), subtract the result from (8), and write the result into the matrix form, yielding

$$\dot{\boldsymbol{x}}_i(t) = \boldsymbol{A}_{i,i}\boldsymbol{x}_i(t) + \sum_{j=p}^{i-1} \boldsymbol{A}_{i,j}\boldsymbol{x}_i(t-\sigma_i), \tag{22}$$

where $\boldsymbol{A}_{i,i}$ and $\boldsymbol{A}_{i,j}$ $(j = p, \ldots, i-1)$ are given in (14). Applying the Newton–Leibniz formula, we obtain

$$\boldsymbol{x}_i(t-\sigma_i) = \boldsymbol{x}_i(t) - \int_{t-\sigma_i}^{t} \dot{\boldsymbol{x}}_i(\tau)\mathrm{d}\tau\,. \tag{23}$$

Substituting this into (22) yields

$$\dot{\boldsymbol{x}}_i(t) = \sum_{k=p}^{i} \boldsymbol{A}_{i,k}\boldsymbol{x}_i(t) - \sum_{j=p}^{i-1} \boldsymbol{A}_{i,j}\int_{t-\sigma_i}^{t} \dot{\boldsymbol{x}}_i(\tau)\mathrm{d}\tau\,. \tag{24}$$

To prove the internal stability of time-delayed systems with switching connectivity topologies, we leverage the Lyapunov–Krasovskii approach [29]. That is, one needs to construct a single positive definite functional, of which the time derivative is always negative definite for all possible connectivity topologies. Here, we use the functional

$$\begin{aligned} \mathscr{L} = {} & \boldsymbol{x}_i^{\mathrm{T}}(t)\boldsymbol{P}\boldsymbol{x}_i(t) + \int_{t-\sigma_i}^{t} \boldsymbol{x}_i^{\mathrm{T}}(\tau)\boldsymbol{Q}\boldsymbol{x}_i(\tau)\mathrm{d}\tau \\ & + \int_{-\sigma_i}^{0}\int_{t+\theta}^{t} \dot{\boldsymbol{x}}_i^{\mathrm{T}}(\tau)\boldsymbol{W}\dot{\boldsymbol{x}}_i(\tau)\mathrm{d}\tau\mathrm{d}\theta, \end{aligned} \tag{25}$$

where $\boldsymbol{P}, \boldsymbol{Q}, \boldsymbol{W}$ are all positive definite matrices such that the functional $\mathscr{L}$ is also positive definite.

Differentiating (25) with respect to time leads to

$$\begin{aligned} \dot{\mathscr{L}} = {} & \dot{\boldsymbol{x}}_i^{\mathrm{T}}(t)\boldsymbol{P}\boldsymbol{x}_i(t) + \boldsymbol{x}_i^{\mathrm{T}}(t)\boldsymbol{P}\dot{\boldsymbol{x}}_i(t) + \boldsymbol{x}_i^{\mathrm{T}}(t)\boldsymbol{Q}\boldsymbol{x}_i(t) \\ & - \boldsymbol{x}_i^{\mathrm{T}}(t-\sigma_i)\boldsymbol{Q}\boldsymbol{x}_i(t-\sigma_i) + \sigma_i\dot{\boldsymbol{x}}_i^{\mathrm{T}}(t)\boldsymbol{W}\dot{\boldsymbol{x}}_i(t) \\ & - \int_{t-\sigma_i}^{t} \dot{\boldsymbol{x}}_i^{\mathrm{T}}(\tau)\boldsymbol{W}\dot{\boldsymbol{x}}_i(\tau)\mathrm{d}\tau\,. \end{aligned} \tag{26}$$

To make the subsequent expressions more compact, we define

$$\boldsymbol{\chi}(t,\tau) = \begin{bmatrix} \boldsymbol{x}_i(t) \\ \boldsymbol{x}_i(t-\sigma_i) \\ \dot{\boldsymbol{x}}_i^{\mathrm{T}}(\tau) \end{bmatrix}. \tag{27}$$

Substituting (22) and (24) into (26), and considering the identity

$$\boldsymbol{x}^{\mathrm{T}}(t)\boldsymbol{A}\boldsymbol{x}(t) = \frac{1}{\sigma_i}\int_{t-\sigma_i}^{t} \boldsymbol{x}^{\mathrm{T}}(t)\boldsymbol{A}\boldsymbol{x}(t)\mathrm{d}\tau \tag{28}$$

in the result, we obtain

$$\dot{\mathscr{L}} = \int_{t-\sigma_i}^{t} \boldsymbol{\chi}_i^{\mathrm{T}}(t,\tau)\boldsymbol{\Xi}\boldsymbol{\chi}_i(t,\tau)\mathrm{d}\tau, \tag{29}$$

where the matrix $\boldsymbol{\Xi}$ is given in (12). If $\boldsymbol{\Xi}$ is negative definite, $\chi_i^{\mathrm{T}}(t,\tau)\boldsymbol{\Xi}\chi_i(t,\tau)$ is also negative definite for all $t-\sigma_i \le \tau \le t$. Note that the integration does not change the negative sign, $\dot{\mathscr{L}}$ is always negative definite, which completes the proof.

7.2 Physics-based vehicle dynamic model

The physics-based longitudinal dynamic model is given by [30] in the form

$$\begin{aligned}\dot{\bar{s}}_i &= \bar{v}_i,\\ \dot{\bar{v}}_i &= -\frac{mg}{m_{\mathrm{eff}}}\sin\phi_i - \frac{rmg}{m_{\mathrm{eff}}}\cos\phi_i\\ &\quad -\frac{k}{m_{\mathrm{eff}}}(\bar{v}_i+v_{\mathrm{w}})^2 + \frac{1}{m_{\mathrm{eff}}R}T_{\mathrm{a},i},\end{aligned} \tag{30}$$

where $\bar{s}_i$ and $\bar{v}_i$ denote the real position and real velocity of vehicle i. The effective mass $m_{\mathrm{eff}} = m + J/R^2$ is determined by the vehicle mass m, the moment of inertia J of the rotating elements, and the wheel radius R. g, r, and k represent the gravitational constant, rolling resistance coefficient, and aerodynamic drag coefficient, respectively. ϕ_i and v_{w} denote the road grade and headwind speed, respectively. When implementing CACC through the hierarchical control architecture presented in [15], the axle torque $T_{\mathrm{a},i}$ is designed to regulate the vehicle states $\bar{s}_i$ and $\bar{v}_i$ to track the desired states s_i and v_i given by (8), respectively.

In the simulation, we use the following parameters in the model (30). The mass $m = 1500$ kg, the aerodynamic drag coefficient $k = 0.3$ kg/m, the tire radius $R = 0.5$ m, the tire rolling resistance coefficient $r = 0.006$, the rotational inertia $J = 5\,\mathrm{kg\,m^2}$, and gravitational constant $g = 9.81$ m/s^2.